Nano Research

Open Access

Research Article

ZnSeTe/CdZnSe-based type-II core–shell quantum dots with tunable blue emission

Muhammad Ramzan[1], Chenhui Wang[2] ✉, Mingrui Liu[1], Peng Huang[3], Jing Li[4], Yin Song[3], and Haizheng Zhong[1] ✉

[1] *MIIT Key Laboratory for Low-Dimensional Quantum Structure and Devices, School of Materials Science and Engineering, Beijing Institute of Technology, Beijing 100081, China*
[2] *Beijing Engineering Research Center for Mixed Reality and Advanced Display Technology, School of Optics and Photonics, Beijing Institute of Technology, Beijing 100081, China*
[3] *MIIT Key Laboratory of Complex-Field Intelligent Exploration, School of Optics and Photonics, Beijing Institute of Technology, Beijing 100081, China*
[4] *Key Laboratory of Photochemical Conversion and Optoelectronic Materials, Technical Institute of Physics and Chemistry, Chinese Academy of Sciences, Beijing 100190, China*

Cite this article: *Nano Research*, **2025**, *18*, 94907267. https://doi.org/10.26599/NR.2025.94907267

ABSTRACT: Blue emissive quantum dots are key materials in emerging light-emitting technologies for display applications. Herein, we report the synthesis of ZnSeTe/CdZnSe-based type-II core–shell quantum dots with a low Cd content of less than 2.5%. By modifying the Cd content of the CdZnSe shell, photoluminescence emission can be tuned from 430 to 510 nm with a full width at half maximum of less than 26 nm. Transient absorption spectra illustrate the charge transfer between the conduction band of ZnSeTe and the conduction band of CdZnSe, as well as the recombination between the valence band of ZnSeTe and the conduction band of CdZnSe. By subsequent growth of ZnSe and ZnS shells, the resulting quantum dots achieved a photoluminescence quantum yield of 95%. We further demonstrate a blue quantum dot light-emitting diode with an emission peak at 467 nm, showing a maximum external quantum efficiency of 5%, a maximum luminance of 10,376 cd·m^{-2}, and an extrapolated T_{95} lifetime of 4.7 h.

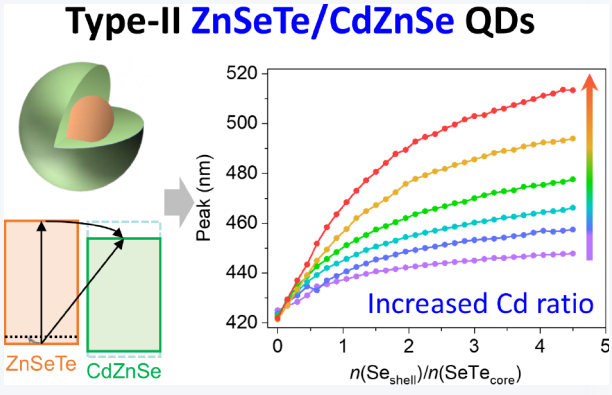

KEYWORDS: quantum dot, blue emission, type-II, light-emitting diode, display

1 Introduction

Quantum dot (QD)-based electroluminescence (EL) technology is recognized as a dependable alternative for upgrading display technologies, primarily due to its high color purity, high efficiency, and solution processability [1–3]. To date, the performance of blue QD light-emitting diodes (QLEDs), particularly their lifetime, lags far behind their red and green counterparts [4–13]. Additionally, the toxicity of Cd is also a limiting factor for further commercialization [14, 15]. So far, the most excellent Cd-free blue emissive QD material is ZnSeTe [7, 16–20]. The devices based on ZnSeTe QDs exhibited an external quantum efficiency (EQE) of over 20% and a T_{95} lifetime of over 30 h [7]. However, these QDs usually face the problem of spectral broadening and tailing due to the presence of Te states, which adversely affects color purity [21]. In(Ga)P QDs [22, 23] and large ZnSe QDs [24–26] are being fabricated as better alternatives of Cd-free materials with high photoluminescence (PL) efficiency. However, these QDs with pure-blue emission still suffer from the challenge of size control, low efficiency, and low operational stability in the application of QLEDs [21, 24, 26–31]. Therefore, developing blue emissive QD materials and devices with low Cd components is crucial for promoting their broader application.

Type-II structure brings more possibilities for tuning the emission of core–shell QDs [32–37]. However, till now, there are only a few reports demonstrating the use of type-II QDs in EL devices [38–41]. Recently, our group reported the synthesis of ZnSe/CdZnS-based type-II QDs emitting in the blue region [42]. In

Received: November 20, 2024; **Revised:** January 21, 2025
Accepted: January 22, 2025

✉Address correspondence to Chenhui Wang, chwang@bit.edu.cn; Haizheng Zhong, hzzhong@bit.edu.cn

this work, for the first time, we report the synthesis of ZnSeTe/CdZnSe-based type-II core–shell QDs. By optimizing the Cd content of the CdZnSe shell, the PL spectra can be tuned in the region of 430–510 nm. With further growth of a ZnSe shell, the full width at half maximum (FWHM) can be decreased to less than 22 nm. The formation of the type-II structure was justified by transient absorption (TA) analyses. Furthermore, we demonstrate blue QLEDs with a maximum EQE of 5%, a maximum luminance of 10,376 cd·m^{-2}, and an extrapolated T_{95} lifetime of 4.7 h.

2 Results and discussion

The synthesis route of $ZnSe_{0.975}Te_{0.025}/Cd_{0.18}Zn_{0.82}Se/ZnSe/ZnS$ QDs is illustrated in Fig. 1(a). Typically, $ZnSe_{0.975}Te_{0.025}$ cores were prepared by injecting Se-diphenylphosphine (Se-DPP) and Te-trioctylphosphine (Te-TOP) precursors into Zn oleate ($Zn(OA)_2$) precursors, followed by continuous injection of $Zn(OA)_2$, $Cd(OA)_2$ with Se-TOP precursors for the growth of $Zn_{0.82}Cd_{0.18}Se$ shells, and $Zn(OA)_2$ with Se-TOP or S-TOP precursors for the ZnSe and ZnS shells. Figure 1(b) shows the evolution of PL and absorption spectra during the synthesis. The $ZnSe_{0.975}Te_{0.025}$ cores exhibited a PL emission with a FWHM of 31 nm at 424 nm. After the growth of $Cd_{0.18}Zn_{0.82}Se$ shell, the emission peak red-shifted to 459 nm, and the FWHM decreased to 25 nm. Further growth of ZnSe and ZnS shells resulted in a final peak of 463 nm with a FWHM of 18 nm. The PLQYs were enhanced by the growth of the shell on $ZnSe_{0.975}Te_{0.025}$ cores with a maximum value of 95% after coating the ZnS shell. Transmission electron microscopy (TEM) characterizations revealed that the size of $ZnSe_{0.975}Te_{0.025}$ cores was 4.9 nm (Fig. 1(c) and Fig. S1(a) in the Electronic Supplementary Material (ESM)). By coating the $Cd_{0.18}Zn_{0.82}Se$ shell, the size was increased to 6.7 nm (Fig. 1(d) and Fig. S1(b) in the ESM), and further increased to 8.7 nm with the ZnSe and ZnS shells (Fig. 1(e) and Fig. S1(c) in the ESM). Energy dispersive spectroscopy (EDS) and inductively coupled plasma optical emission spectroscopy (ICP-OES) characterizations revealed that the Cd mass fractions of the $ZnSe_{0.975}Te_{0.025}/Cd_{0.18}Zn_{0.82}Se/ZnSe/ZnS$ QDs are 1.32% and 2.16%, respectively, suggesting a relatively low Cd content compared to the currently reported blue QDs (Fig. S2 and Table S1 in the ESM) [8]. X-ray diffraction (XRD) analyses revealed that the core, C/S, and C/S/S/S QDs have a zinc blend crystal structure (Fig. 1(f)).

We investigated the PL evolution of $Cd_xZn_{1-x}Se$ shell growth on $ZnSe_{0.975}Te_{0.025}$ cores with various Cd content. As shown in Figs. 2(a) and 2(b), and Fig. S3 in the ESM, the growth of ZnSe shell on the $ZnSe_{0.975}Te_{0.025}$ cores resulted in a gradual redshift from 425 to 448 nm, accompanied by an obvious decrease of FWHM from 37 to 17 nm [7]. As the amount of Cd of $Cd_xZn_{1-x}Se$ shell increased, a noticeable redshift occurred, and the FWHM also became narrower compared to $ZnSe_{0.975}Te_{0.025}$ core. The $Cd_{0.3}Zn_{0.7}Se$ shell growth on $ZnSe_{0.975}Te_{0.025}$ core led to a peak wavelength exceeding 500 nm, with a redshift of more than 87 nm and an FWHM reduced to below 26 nm. The substantial peak redshift, dependent on Cd content, suggests the formation of a type-II structure between $ZnSe_{0.975}Te_{0.025}$ core and $Cd_xZn_{1-x}Se$ shell. By growing an outer ZnSe shell, the FWHM of the type-II core–shell QDs can be further decreased. We fabricated three typical QDs with emission peaks centered at 446, 458, and 470 nm by changing the Cd content (6%, 18%, and 30%, respectively) and thickness of $Cd_xZn_{1-x}Se$ shell. As shown in Figs. 2(c) and 2(d), and Fig. S4 in the ESM, all the three QDs showed a redshift of a few nanometers with the coating of ZnSe shell, but showed a significant continuous decrease of FWHM to below 22 nm. These results suggested that these ZnSeTe/CdZnSe type-II core–shell QDs are emission-tunable within the region from 430 to 510 nm with high color purity.

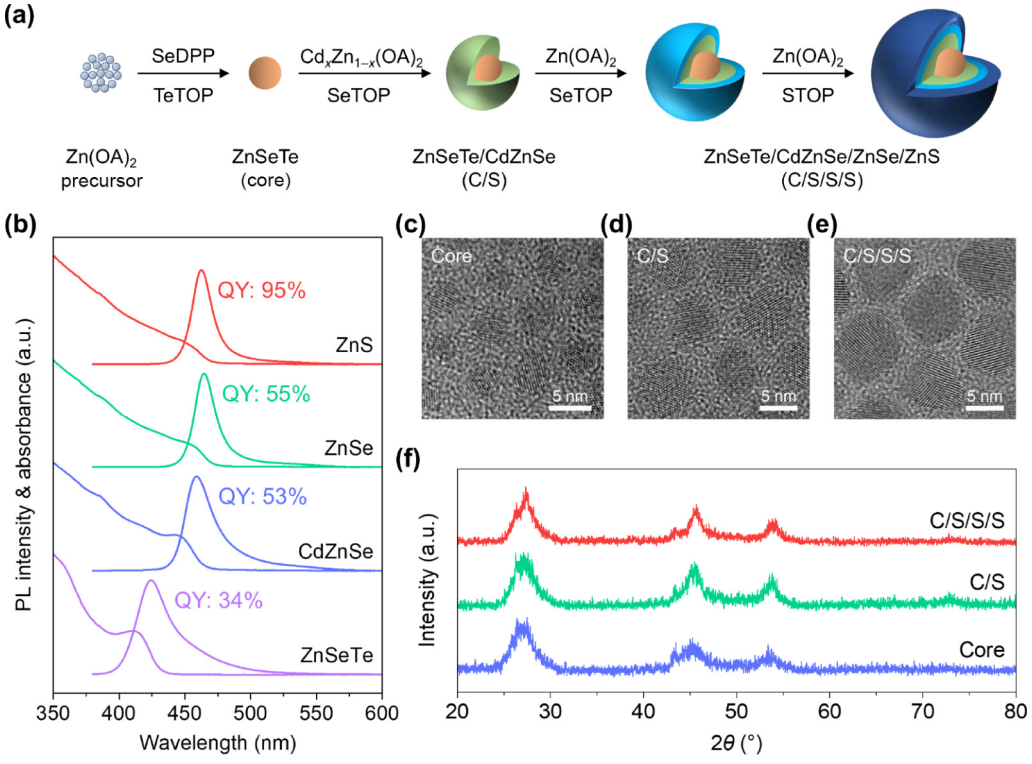

Figure 1 Synthetic route and characterizations of $ZnSe_{0.975}Te_{0.025}/Cd_{0.18}Zn_{0.82}Se/ZnSe/ZnS$ QDs. (a) The schematic synthetic route of the QDs. (b) PL and absorption spectra of the QDs during the synthesis. TEM images of (c) $ZnSe_{0.975}Te_{0.025}$ (core), (d) $ZnSe_{0.975}Te_{0.025}/Cd_{0.18}Zn_{0.82}Se$ (C/S), and (e) $ZnSe_{0.975}Te_{0.025}/Cd_{0.18}Zn_{0.82}Se/ZnSe/ZnS$ (C/S/S/S) QDs. Scale bar, 5 nm. (f) XRD patterns of the core, C/S, and C/S/S/S QDs.

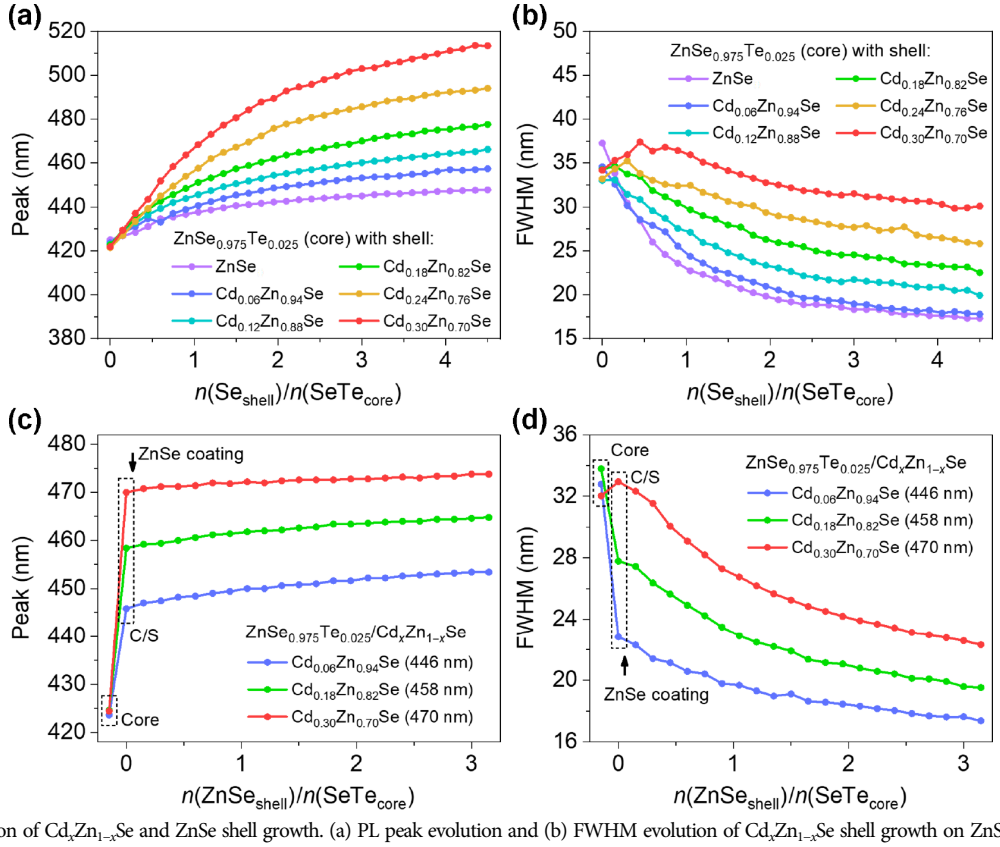

Figure 2 PL evolution of $Cd_xZn_{1-x}Se$ and ZnSe shell growth. (a) PL peak evolution and (b) FWHM evolution of $Cd_xZn_{1-x}Se$ shell growth on $ZnSe_{0.975}Te_{0.025}$ cores with various Cd content. (c) PL peak evolution and (d) FWHM evolution of ZnSe shell growth on $ZnSe_{0.975}Te_{0.025}/Cd_xZn_{1-x}Se$ core–shell QDs.

To verify the type-II structure of $ZnSe_{1-y}Te_y/Cd_xZn_{1-x}Se$ core–shell QDs, we conducted TA measurements with different Cd ratio and Te ratios. Figure 3(a) shows the band structure of ZnSeTe/ZnSe QDs. The positions of each transition were analyzed by TA spectra and the second derivative of the absorption spectra (Fig. S5 in the ESM). As shown in Fig. 3(c), three bleaching peaks at 375, 429, and 443 nm (denoted as A, B, and C, respectively) were observed in TA spectra of $ZnSe_{0.95}Te_{0.05}$/ZnSe QDs, which were assigned as respective $1S_e$–$1S_h$, $1S_e$–$2S_h$, and $1P_e$–$1P_h$ transition [43–45]. According to the literature report, Te doping in ZnSe induces localized hole states above the valance band maximum (VBM) of ZnSe, resulting in the relaxation of hot-carrier in several hundred femtoseconds, with a slight contribution to the conduction band maximum (CBM) of ZnSe [46]. The typical band edge alignment of $ZnSe_{0.95}Te_{0.05}$/ZnSe is shown in the first figure of Fig. 3(b). As shown in Figs. 3(d)–3(f), when coating $Cd_xZn_{1-x}Se$ shell on the $ZnSe_{0.95}Te_{0.05}$ core, the peak at 375 nm split into two peaks: One is located at 375 nm (denoted as A_1) which does not change with the increase of Cd content, meanwhile the other one is observed in the longer wavelength region from A_1 (denoted as A_2) and red-shifts with the increase of Cd content (383 nm for x = 0.12, 395 nm for x = 0.24, 409 nm for x = 0.36, respectively). In addition, the peaks of B and C gradually red-shift (denoted as B' and C', respectively) with the increase of Cd content (430 and 450 nm for x = 0.12, 442 and 469 nm for x = 0.24, 456 and 485 nm for x = 0.36, respectively). The decreased energy of the three typical transitions (A_2, B', and C') indicates that the band alignments have been tuned, and such changes are correlated with the Cd content of the shell.

Since the introduction of alloyed Cd atom in ZnSe results in a significant decreased in the energy of the CBM and VBM (with greater contribution to CBM), we attribute the above changes of the typical transitions to the formation of type-II structures between $ZnSe_{0.95}Te_{0.05}$ core and $Cd_xZn_{1-x}Se$ shell. Specifically, Cd alloying in the ZnSe shell induces a significant reduction in the energy of the CBM of ZnSe, and the band-edge recombination is formed from the CBM of $Cd_xZn_{1-x}Se$ shell to the VBM as well as Te states of $ZnSe_{0.95}Te_{0.05}$ core. This was further proved by the TA kinetic analyses. As shown in Fig. 3(i), the normalized TA kinetics of $ZnSe_{0.95}Te_{0.05}/Cd_xZn_{1-x}Se$ QDs with various Cd content show that the A_1 bleaching signal at 373 nm experienced a faster decay with the increase of Cd content in $Cd_xZn_{1-x}Se$ shell. This kinetic can be assigned to the excitation of $ZnSe_{0.95}Te_{0.05}$ core with following fast transition from the CB of $ZnSe_{0.95}Te_{0.05}$ core to the $Cd_xZn_{1-x}Se$ shell. The type-II structures and the typical transition processes are shown in the second and third figures of Fig. 3(b).

We further analyzed the influence of Te on the type-II structure of $ZnSe_{1-y}Te_y/Cd_{0.24}Zn_{0.76}Se$ QDs. As shown in Figs. 3(g), 3(e), and 3(h), with the increase of Te content from 2.5% to 5% and 10%, both A_1 and A_2 signal positions remain at 375 and 395 nm, and the TA kinetics of A_1 and A_2 bleaching signals show similar characterizations (Fig. 3(j)). These results suggest that Te content shows no effects on the transition from $1P_h$ of $ZnSe_{1-y}Te_y$ core to the CB of $Cd_{0.24}Zn_{0.76}Se$ shell (the fourth figure of Fig. 3(b)). In addition, B' and C' signal positions gradually red-shift, suggesting the subsequent transition of hot-carrier and the recombination contributed by the localized Te states of $ZnSe_{1-y}Te_y$ core with CB of $Cd_{0.24}Zn_{0.76}Se$ shell. As shown in Fig. S6 in the ESM, we demonstrate that the PL emission can also be tuned by varying the Te ratio (peak of 472 nm for 2.5%, 483 nm for 5%, and 505 nm for 10%), however, the increase of Te content results in broader spectra (FWHM of 24 nm for 2.5%, 38 nm for 5%, and 57 nm for 10%).

We fabricated QLEDs with a structure of indium tin oxide

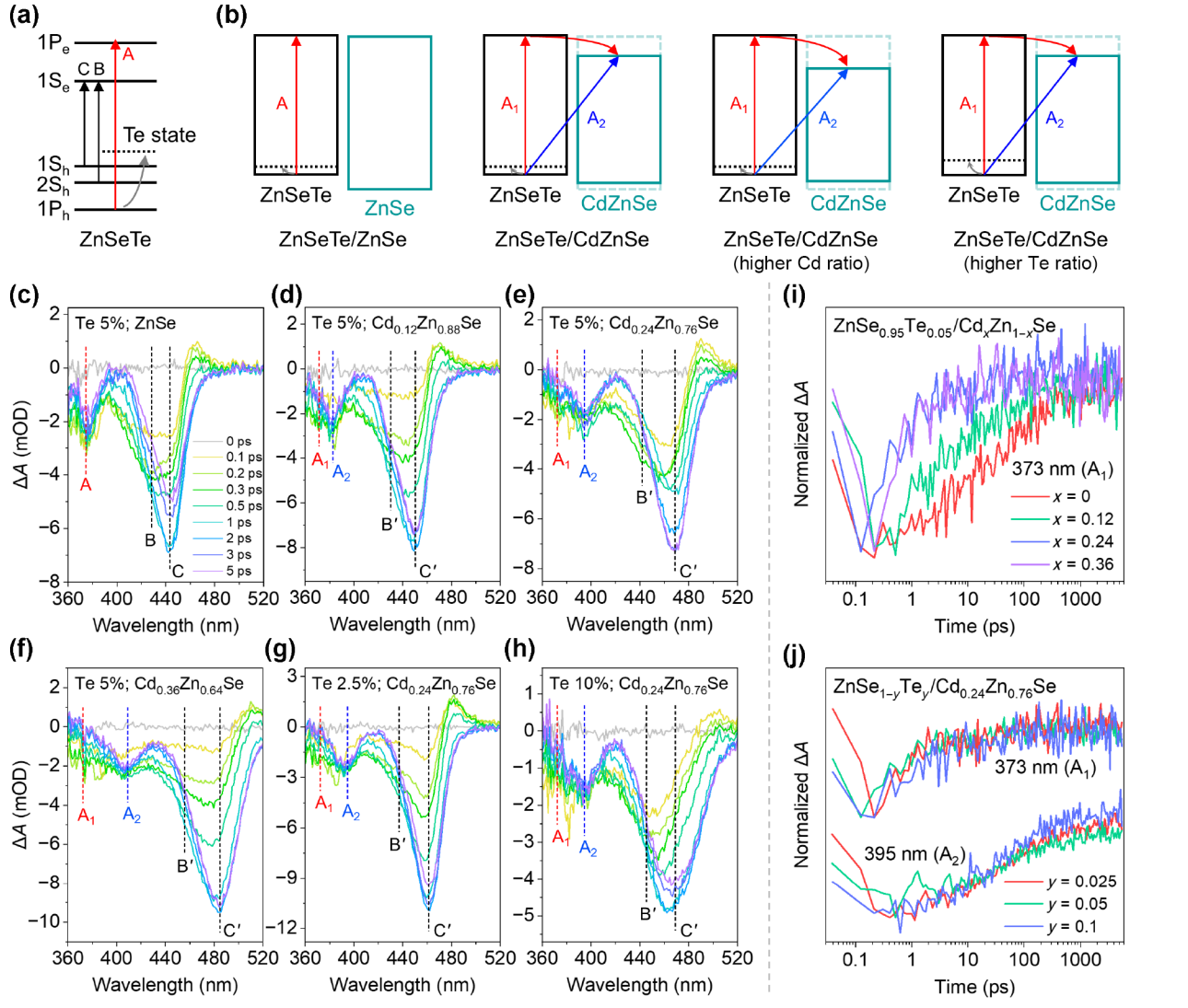

Figure 3 Type-II band structure analyses of ZnSeTe/CdZnSe QDs. (a) Schematic diagram of energy level with the transitions of ZnSeTe/ZnSe QDs. (b) Schematic diagram of band structure with the transitions of ZnSeTe/CdZnSe QDs. TA spectra at various delay times for $ZnSe_{1-y}Te_y/Cd_xZn_{1-x}Se$ QDs with various Cd and Te content: (c) $x = 0$, $y = 0.05$; (d) $x = 0.12$, $y = 0.05$; (e) $x = 0.24$, $y = 0.05$; (f) $x = 0.36$, $y = 0.05$; (g) $x = 0.24$, $y = 0.025$; and (h) $x = 0.24$, $y = 0.1$. (i) TA kinetics of the peak A_1 (373 nm) of $ZnSe_{0.95}Te_{0.05}/Cd_xZn_{1-x}Se$ QDs with various Cd content. (j) TA kinetics of the peaks A_1 (373 nm) and A_2 (395 nm) of $ZnSe_{1-y}Te_y/Cd_{0.24}Zn_{0.76}Se$ QDs with various Te content.

(ITO)/poly(3,4-ethylenedioxythiophene):poly(styrenesulfonate) (PEDOT:PSS)/poly((9,9-dioctylfluorenyl-2,7-diyl)-co-(4,4'-(N-(4-sec-butylphenyl)diphenylamine))(TFB)/QDs/ZnMgO/aluminum (Al), as shown in Fig. 4(a). The devices were encapsulated with an acid-free ultraviolet curable resin without any post-treatment before testing. The EL spectra under various forward biased peaks at 467 nm with a FWHM of 24 nm (Fig. 4(b)), corresponding to the Commission Internationale de l'Eclairage (CIE) color coordinates of (0.13, 0.12). The current density–luminance–voltage and EQE–current density curves of the devices are shown in Figs. 4(c) and 4(d). The device exhibits a sub-bandgap turn-on voltage at 2.2 V with the luminance of 1 cd·m^{-2} (Fig. 4(c)), indicating an efficient electron and hole injection. A maximum luminance of 10,376 cd·m^{-2} is achieved at 7.2 V with a current density of 320.2 mA·cm^{-2} (Fig. 4(c)), and a maximum EQE of 5.0% is achieved at 3.8 V with a luminance of 1293 cd·m^{-2} (Fig. 4(d)). A histogram of EQEs for 30 devices shows an average value of 4.4% (Fig. S7 in the ESM), indicating the good reproducibility. Furthermore, we conducted operational stability test. The blue QLED shows a T_{95} lifetime of 6.2 h at the initial luminance of 854 cd·m^{-2}, which can be extrapolated to 4.7 h at 1000 cd·m^{-2} (Fig. S8 in the ESM).

3 Conclusion

Hence, we report the synthesis of ZnSeTe/CdZnSe-based QDs with a type-II structure. With the change of Cd content, PL emission can be tuned in the region of 430–510 nm with a FWHM of less than 26 nm. These ZnSeTe/CdZnSe type-II core–shell QDs have a low Cd content of less than 2.5%. As indicated by the TA analyses, the blue emission originates from the recombination between the VB of ZnSeTe core and the CB of CdZnSe shell. By further shell coating, the $ZnSe_{0.975}Te_{0.025}/Cd_{0.18}Zn_{0.82}Se$/ZnSe/ZnS QDs exhibited a high PLQY of 95%. The QLED based on these QDs exhibited a maximum EQE of 5%, a maximum luminance of 10,376 cd·m^{-2}, and an extrapolated T_{95} lifetime of 4.7 h. In all, the type-II core–shell QDs are alternative blue emitters to promote the development of QLEDs for display applications.

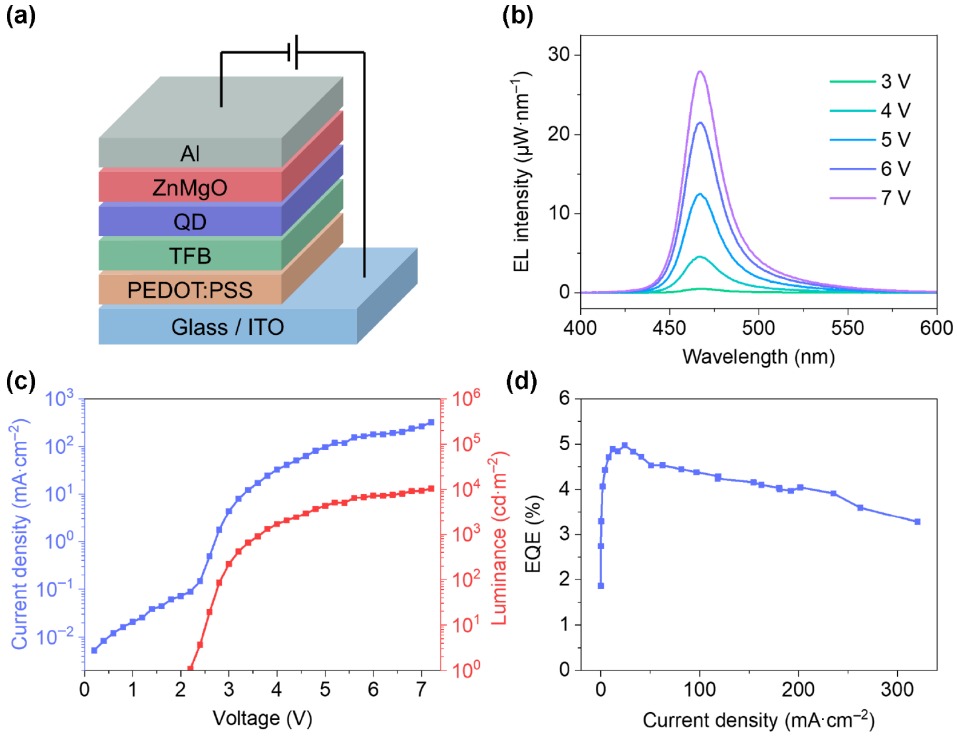

Figure 4 Characteristics of the best-performance blue QLED. (a) Device structure diagram. (b) EL spectra at various voltage. (c) Current density–luminance–voltage curves. (d) EQE–current density curve.

4 Experimental section

4.1 Materials

Zinc acetate ($ZnAc_2$, 99.99%), CdO (99.99%), Se (99.99%), Te (99.8%), S (99.998%), oleic acid (OA, 90%), 1-octadecene (ODE, 90%), TOP (97%), zinc acetate dihydrate ($ZnAc_2{\cdot}2H_2O$, 99.999%), tetramethylammonium hydroxide pentahydrate ($TMAH{\cdot}5H_2O$, 97%), dimethyl sulfoxide (DMSO, anhydrous, 99.9%), chlorobenzene (anhydrous, 99.8%), ethanol (anhydrous, 99.5%), and octane (anhydrous, 99%) were purchased from Sigma-Aldrich. DPP (95%) was purchased from Aladdin. PEDOT:PSS was purchased from Xi'an Polymer Light Technology Corp. TFB was purchased from American Dye Source.

4.2 Preparation of precursor solutions

Se-DPP precursor was prepared in a nitrogen-filled glove box by dissolving 0.4 mmol Se in 1 mL DPP. Te-TOP precursor was prepared in a nitrogen-filled glove box by dissolving 0.01 mmol Te in 1 mL TOP. Se-TOP precursor was prepared in a nitrogen-filled glove box by dissolving 20 mmol Se in 10 mL TOP. S-TOP precursor was prepared in a nitrogen-filled glove box by dissolving 20 mmol S in 10 mL TOP. $Zn(OA)_2$ precursor was prepared in a three-neck flask by dissolving 20 mmol $ZnAc_2$ in 20 mL OA and 20 mL ODE, and degassed at 120 °C under vacuum for 1 h. $Cd(OA)_2$ precursor was prepared in a three-neck flask by dissolving 20 mmol CdO in 20 mL OA and 20 mL ODE, and degassed at 120 °C under vacuum for 30 min, followed by reaction at 250 °C for 1 h. The $Zn(OA)_2$ and $Cd(OA)_2$ precursor solutions were kept at 80 °C under argon for further use.

4.3 Synthesis of QDs

0.5 mmol $ZnAc_2$ with 1 mL OA and 8 mL ODE in a 50 mL three-neck flask were degassed at 120 °C under vacuum for 1 h, followed by heating at 300 °C under argon. Then, 0.5 mL Se-DPP mixed with 0.51 mL Te-TOP was swiftly injected into the flask and reacted for 40 min. For the $Zn_{0.82}Cd_{0.18}Se$ shell, a mixture of 0.492 mL $Zn(OA)_2$, 0.108 mL $Cd(OA)_2$, and 0.15 mL Se-TOP precursor was injected at a rate of 3 $mL{\cdot}h^{-1}$. For the ZnSe shell, a mixture of 0.8 mL $Zn(OA)_2$ and 0.2 mL Se-TOP precursor was injected at a rate of 3 $mL{\cdot}h^{-1}$. For the ZnS shell, a mixture of 0.4 mL $Zn(OA)_2$ and 0.1 mL S-TOP precursor was injected at a rate of 2 $mL{\cdot}h^{-1}$. The solution was then cooled to room temperature, followed by purification with ethanol and hexane.

4.4 Synthesis of ZnMgO nanocrystals

Colloidal $Zn_{0.9}Mg_{0.1}O$ QDs were synthesized by dropping an ethanol solution (10 mL) of $TMAH{\cdot}5H_2O$ (5 mmol) into a DMSO solution (30 mL) of $ZnAc_2{\cdot}2H_2O$ (2.7 mmol) and $MgAc_2{\cdot}4H_2O$ (0.3 mmol), followed by stirring for 1 h. Then the QDs were purified from the solution with ethyl acetate and dispersed in ethanol.

4.5 Device fabrication

The patterned ITO substrates were sequentially cleaned with deionized water, acetone, ethanol, and isopropanol in an ultrasonic bath. The dried substrates were treated under oxygen plasma etching for 3 min. PEDOT:PSS was first spin-coated onto the substrates at 4000 rpm for 40 s and baked at 150 °C for 20 min in air, then the samples were transferred into a nitrogen-filled glove box ($O_2 \leq 1$ ppm, $H_2O \leq 1$ ppm). TFB (in chlorobenzene, 8 $mg{\cdot}mL^{-1}$) was spin-coated at 2000 rpm for 40 s and baked at 150 °C for 30 min. Blue QDs (in octane, 18 $mg{\cdot}mL^{-1}$) were spin-coated at 2000 rpm for 40 s. $Zn_{0.9}Mg_{0.1}O$ nanocrystals (30 $mg{\cdot}mL^{-1}$) were spin-coated at 3000 rpm for 40 s and baked at 80 °C for 20 min. Finally, Al (100 nm) was deposited by thermal evaporation

under a high vacuum of 10^{-4} Pa. The devices were encapsulated in a glove box by using an acid-free ultraviolet curable resin (LOCTITE 3335), followed by annealing at 80 °C for 30 min. The active area of the device was 4 mm^2.

4.6 Characterization

Steady-state PL spectra were recorded on a Tianjin Gangdong F-380 fluorescence spectrometer (excitation: 365 nm). Steady-state ultraviolet–visible (UV–vis) absorption spectra were recorded on a Mapada UV-6100 UV–vis spectrophotometer. The PLQYs of the films were tested by using a Hamamatsu C9920-02 absolute PLQY measurement system composed of a PMA-12 photonic multichannel analyzer and an integrating sphere (excitation: 365 nm). TEM and EDS images were recorded on a FEI Tecnai G2 F30 transmission electron microscopy. ICP–OES measurements were conducted using a Thermo Scientific iCAP 7200 ICP–OES spectrophotometer. XRD patterns were recorded on a Bruker D8 Advance X-ray diffractometer with a Cu Kα radiation source (λ = 1.5406 Å). TA measurements were carried out at room temperature using a Helios pump–probe system (Ultrafast Systems) combined with a regenerative-amplified Ti:sapphire laser system (Legend Elite-1K-HE, 800 nm, 25 fs, 4 mJ·$pulse^{-1}$, and 1 kHz repetition rate) and an optical parametric amplifier system. The wavelength of the pump pulse was 350 nm. Current density–voltage–luminance characteristics and EL spectra were measured with a system consisting of a digital source meter (Keithley 2400) and an integrating sphere (FOIS, Ocean Optics) coupled to a spectrometer (QE Pro, Ocean Optics). The absolute spectral radiant flux is calibrated by using a NIST-traceable radiant-flux standard lamp (HL-3 plus, Ocean Optics). The EQEs of the devices were calculated with the assumption of Lambertian emission pattern, according to the previously reported method [47].

Electronic Supplementary Material: Supplementary material (TEM images, integrated EDS spectra, PL spectra, and absorption spectra) is available in the online version of this article at https://doi.org/10.26599/NR.2025.94907267 .

Data availability

All data needed to support the conclusions in the paper are presented in the manuscript and the Electronic Supplementary Material. Additional data related to this paper may be requested from the corresponding author upon request.

Acknowledgements

This work is granted by the National Natural Science Foundation of China (Nos. U23A20683 and 52403291), Natural Science Foundation of Beijing Municipality (No. Z210018), and China Postdoctoral Science Foundation (No. 2024M764129).

Declaration of competing interest

All the contributing authors report no conflict of interests in this work.

Author contribution statement

M. R.: Data curation, experimental design, writing manuscript. C. H. W.: Data analyses, funding acquisition, writing manuscript. M. R. L.: Data analyses. P. H.: Data analyses. J. L.: Test resource provision. Y. S.: Data analyses. H. Z. Z.: Project administration, funding acquisition, data analyses, writing manuscript. All the authors have approved the final manuscript.

Use of AI statement

None.

References

[1] Shirasaki, Y.; Supran, G. J.; Bawendi, M. G.; Bulović, V. Emergence of colloidal quantum-dot light-emitting technologies. *Nat. Photonics* **2013**, *7*, 13–23.

[2] Shu, Y. F.; Lin, X.; Qin, H. Y.; Hu, Z.; Jin, Y. Z.; Peng, X. G. Quantum dots for display applications. *Angew. Chem., Int. Edit.* **2020**, *59*, 22312–22323.

[3] Jang, E.; Jang, H. Review: Quantum dot light-emitting diodes. *Chem. Rev.* **2023**, *123*, 4663–4692.

[4] Dai, X. L.; Zhang, Z. X.; Jin, Y. Z.; Niu, Y.; Cao, H. J.; Liang, X. Y.; Chen, L. W.; Wang, J. P.; Peng, X. G. Solution-processed, high-performance light-emitting diodes based on quantum dots. *Nature* **2014**, *515*, 96–99.

[5] Shen, H. B.; Gao, Q.; Zhang, Y. B.; Lin, Y.; Lin, Q. L.; Li, Z. H.; Chen, L.; Zeng, Z. P.; Li, X. G.; Jia, Y. et al. Visible quantum dot light-emitting diodes with simultaneous high brightness and efficiency. *Nat. Photonics* **2019**, *13*, 192–197.

[6] Won, Y. H.; Cho, O.; Kim, T.; Chung, D. Y.; Kim, T.; Chung, H.; Jang, H.; Lee, J.; Kim, D.; Jang, E. Highly efficient and stable InP/ZnSe/ZnS quantum dot light-emitting diodes. *Nature* **2019**, *575*, 634–638.

[7] Kim, T.; Kim, K. H.; Kim, S.; Choi, S. M.; Jang, H.; Seo, H. K.; Lee, H.; Chung, D. Y.; Jang, E. Efficient and stable blue quantum dot light-emitting diode. *Nature* **2020**, *586*, 385–389.

[8] Deng, Y. Z.; Peng, F.; Lu, Y.; Zhu, X. T.; Jin, W. X.; Qiu, J.; Dong, J. W.; Hao, Y. L.; Di, D. W.; Gao, Y. et al. Solution-processed green and blue quantum-dot light-emitting diodes with eliminated charge leakage. *Nat. Photonics* **2022**, *16*, 505–511.

[9] Chen, X. T.; Lin, X. F.; Zhou, L. K.; Sun, X. J.; Li, R.; Chen, M. Y.; Yang, Y. X.; Hou, W. J.; Wu, L. J.; Cao, W. R. et al. Blue light-emitting diodes based on colloidal quantum dots with reduced surface-bulk coupling. *Nat. Commun.* **2023**, *14*, 284.

[10] Gao, Y.; Li, B.; Liu, X. N.; Shen, H. B.; Song, Y.; Song, J. J.; Yan, Z. J.; Yan, X. H.; Chong, Y. H.; Yao, R. Y. et al. Minimizing heat generation in quantum dot light-emitting diodes by increasing quasi-Fermi-level splitting. *Nat. Nanotechnol.* **2023**, *18*, 1168–1174.

[11] Xu, H. Y.; Song, J. J.; Zhou, P. H.; Song, Y.; Xu, J.; Shen, H. B.; Fang, S. C.; Gao, Y.; Zuo, Z. J.; Pina, J. M. et al. Dipole–dipole-interaction-assisted self-assembly of quantum dots for highly efficient light-emitting diodes. *Nat. Photonics* **2024**, *18*, 186–191.

[12] Zhang, W. J.; Li, B.; Chang, C.; Chen, F.; Zhang, Q.; Lin, Q. L.; Wang, L.; Yan, J. H.; Wang, F. F.; Chong, Y. H. et al. Stable and efficient pure blue quantum-dot LEDs enabled by inserting an anti-oxidation layer. *Nat. Commun.* **2024**, *15*, 783.

[13] Li, M. Q.; Li, R.; Wu, L. J.; Lin, X. F.; Xia, X. Q.; Ao, Z. T.; Sun, X. J.; Chen, X. T.; Chen, S. Ultrabright and stable top-emitting quantum-dot light-emitting diodes with negligible angular color shift. *Nat. Commun.* **2024**, *15*, 5161.

[14] Derfus, A. M.; Chan, W. C. W.; Bhatia, S. N. Probing the cytotoxicity of semiconductor quantum dots. *Nano Lett.* **2004**, *4*, 11–18.

[15] Kirchner, C.; Liedl, T.; Kudera, S.; Pellegrino, T.; Muñoz Javier, A.; Gaub, H. E.; Stölzle, S.; Fertig, N.; Parak, W. J. Cytotoxicity of colloidal CdSe and CdSe/ZnS nanoparticles. *Nano Lett.* **2005**, *5*, 331–338.

[16] Jang, E. P.; Han, C. Y.; Lim, S. W.; Jo, J. H.; Jo, D. Y.; Lee, S. H.; Yoon, S. Y.; Yang, H. Synthesis of alloyed ZnSeTe quantum dots as

bright, color-pure blue emitters. *ACS Appl. Mater. Interfaces* **2019**, *11*, 46062–46069.
[17] Han, C. Y.; Lee, S. H.; Song, S. W.; Yoon, S. Y.; Jo, J. H.; Jo, D. Y.; Kim, H. M.; Lee, B. J.; Kim, H. S.; Yang, H. More than 9% efficient ZnSeTe quantum dot-based blue electroluminescent devices. *ACS Energy Lett.* **2020**, *5*, 1568–1576.
[18] Bi, Y. H.; Cao, S.; Yu, P.; Du, Z. T.; Wang, Y. J.; Zheng, J. J.; Zou, B. S.; Zhao, J. L. Reducing emission linewidth of pure-blue ZnSeTe quantum dots through shell engineering toward high color purity light-emitting diodes. *Small* **2023**, *19*, 2303247.
[19] Imran, M.; Paritmongkol, W.; Mills, H. A.; Hassan, Y.; Zhu, T.; Wang, Y. K.; Liu, Y.; Wan, H. Y.; Park, S. M.; Jung, E. et al. Molecular-additive-assisted tellurium homogenization in ZnSeTe quantum dots. *Adv. Mater.* **2023**, *35*, 2303528.
[20] Cheng, C. Y.; Yu, B. B.; Huang, F.; Gao, L.; Cao, K. Q.; Zang, P. P.; Zheng, K. B.; Tian, J. J. Near-unity quantum yield ZnSeTe quantum dots enabled by controlling shell growth for efficient deep-blue light-emitting diodes. *Adv. Funct. Mater.* **2024**, *34*, 2313811.
[21] Deng, X. Z.; Zhang, F. J.; Zhang, Y.; Shen, H. B. Heavy-metal-free blue-emitting ZnSe(Te) quantum dots: Synthesis and light-emitting applications. *J. Mater. Chem. C* **2023**, *11*, 14495–14514.
[22] Xie, R. G.; Battaglia, D.; Peng, X. G. Colloidal InP nanocrystals as efficient emitters covering blue to near-infrared. *J. Am. Chem. Soc.* **2007**, *129*, 15432–15433.
[23] Xu, S.; Ziegler, J.; Nann, T. Rapid synthesis of highly luminescent InP and InP/ZnS nanocrystals. *J. Mater. Chem.* **2008**, *18*, 2653–2656.
[24] Gao, M.; Yang, H. W.; Shen, H. B.; Zeng, Z. P.; Fan, F. J.; Tang, B. B.; Min, J. J.; Zhang, Y.; Hua, Q. Z.; Li, L. S.; Ji, B.; Du, Z et al. Bulk-like ZnSe quantum dots enabling efficient ultranarrow blue light-emitting diodes. *Nano Lett.* **2021**, *21*, 7252–7260.
[25] Long, Z. W.; Liu, M. R.; Wu, X. G.; Gu, K.; Yang, G. L.; Chen, Z.; Liu, Y.; Liu, R. H.; Zhong, H. Z. A reactivity-controlled epitaxial growth strategy for synthesizing large nanocrystals. *Nat. Synth.* **2023**, *2*, 296–304.
[26] He, J. H.; Wang, C. H.; Liu, M. R.; Ramzan, M.; Long, Z. W.; Wu, X. G.; Chen, Y.; Zhong, H. Z. Overcoming side reaction effects in the colloidal synthesis of ZnSe/ZnS core/shell quantum dots with an etching strategy. *Nano Res.* **2024**, *17*, 7020–7026.
[27] Yang, X. Y.; Zhao, D. W.; Leck, K. S.; Tan, S. T.; Tang, Y. X.; Zhao, J. L.; Demir, H. V.; Sun, X. W. Full visible range covering InP/ZnS nanocrystals with high photometric performance and their application to white quantum dot light-emitting diodes. *Adv. Mater.* **2012**, *24*, 4180–4185.
[28] Zhang, H.; Ma, X. Y.; Lin, Q. L.; Zeng, Z. P.; Wang, H. Z.; Li, L. S.; Shen, H. B.; Jia, Y.; Du, Z. L. High-brightness blue InP quantum dot-based electroluminescent devices: The role of shell thickness. *J. Phys. Chem. Lett.* **2020**, *11*, 960–967.
[29] Kim, K. H.; Jo, J. H.; Jo, D. Y.; Han, C. Y.; Yoon, S. Y.; Kim, Y.; Kim, Y. H.; Ko, Y. H.; Kim, S. W.; Lee, C. et al. Cation-exchange-derived InGaP alloy quantum dots toward blue emissivity. *Chem. Mater.* **2020**, *32*, 3537–3544.
[30] Zhang, W. D.; Ding, S. H.; Zhuang, W. D.; Wu, D.; Liu, P.; Qu, X. W.; Liu, H. C.; Yang, H. C.; Wu, Z. H.; Wang, K. et al. InP/ZnS/ZnS core/shell blue quantum dots for efficient light-emitting diodes. *Adv. Funct. Mater.* **2020**, *30*, 2005303.
[31] Wu, Z. H.; Liu, P.; Zhang, W. D.; Wang, K.; Sun, X. W. Development of InP quantum dot-based light-emitting diodes. *ACS Energy Lett.* **2020**, *5*, 1095–1106.
[32] Kim, S.; Fisher, B.; Eisler, H. J.; Bawendi, M. Type-II quantum dots: CdTe/CdSe(core/shell) and CdSe/ZnTe(core/shell) heterostructures. *J. Am. Chem. Soc.* **2003**, *125*, 11466–11467.
[33] Ivanov, S. A.; Piryatinski, A.; Nanda, J.; Tretiak, S.; Zavadil, K. R.; Wallace, W. O.; Werder, D.; Klimov, V. I. Type-II core/shell CdS/ZnSe nanocrystals: Synthesis, electronic structures, and spectroscopic properties. *J. Am. Chem. Soc.* **2007**, *129*, 11708–11719.
[34] Li, X. M.; Shen, H. B.; Li, S.; Niu, J. Z.; Wang, H. Z.; Li, L. S. Investigation on type-II Cu_2S–CdS core/shell nanocrystals: Synthesis and characterization. *J. Mater. Chem.* **2010**, *20*, 923–928.
[35] Bang, J.; Park, J.; Lee, J. H.; Won, N.; Nam, J.; Lim, J.; Chang, B. Y.; Lee, H. J.; Chon, B.; Shin, J. et al. ZnTe/ZnSe (core/shell) type-II quantum dots: Their optical and photovoltaic properties. *Chem. Mater.* **2010**, *22*, 233–240.
[36] Tyrakowski, C. M.; Shamirian, A.; Rowland, C. E.; Shen, H. Y.; Das, A.; Schaller, R. D.; Snee, P. T. Bright type II quantum dots. *Chem. Mater.* **2015**, *27*, 7276–7281.
[37] Cao, K. Q.; Yu, B. B.; Huang, F.; Pan, Q. Y.; Wang, J. F.; Ning, J. J.; Zheng, K. B.; Pullerits, T.; Tian, J. J. Constructing ZnTe spherical quantum well for efficient light emission. *Nano Lett.* **2024**, *24*, 5238–5245.
[38] Lin, Q. L.; Song, B.; Wang, H. Z.; Zhang, F. J.; Chen, F.; Wang, L.; Li, L. S.; Guo, F.; Shen, H. B. High-efficiency deep-red quantum-dot light-emitting diodes with type-II CdSe/CdTe core/shell quantum dots as emissive layers. *J. Mater. Chem. C* **2016**, *4*, 7223–7229.
[39] Jin, X.; Li, H. Y.; Huang, S. J.; Gu, X. B.; Shen, H. B.; Li, D. Y.; Zhang, X. G.; Zhang, Q.; Li, F.; Li, Q. H. Bright alloy type-II quantum dots and their application to light-emitting diodes. *J. Colloid Interface Sci.* **2018**, *510*, 376–383.
[40] Karatum, O.; Jalali, H. B.; Sadeghi, S.; Melikov, R.; Srivastava, S. B.; Nizamoglu, S. Light-emitting devices based on type-II InP/ZnO quantum dots. *ACS Photonics* **2019**, *6*, 939–946.
[41] Eren, G. O.; Sadeghi, S.; Jalali, BH. HB.; Ritter, M.; Han, M.; Baylam, I.; Melikov, R.; Onal, A.; Oz, F.; Sahin, M. et al. Cadmium-free and efficient type-II InP/ZnO/ZnS quantum dots and their application for LEDs. *ACS Appl. Mater. Interfaces* **2021**, *13*, 32022–32030.
[42] Liu, M. R.; Wang, C. H.; Huang, P.; He, J. H.; Ramzan, M.; Zhong, H. Z. Pure-blue emissive ZnSe/$Cd_xZn_{1-x}S$/ZnS quantum dots with type-II core–shell structure for display application. *Nano Res.* **2024**, *17*, 10476–10482.
[43] Norris, D. J.; Bawendi, M. G. Measurement and assignment of the size-dependent optical spectrum in CdSe quantum dots. *Phys. Rev. B* **1996**, *53*, 16338–16346.
[44] Lomascolo, M.; Cretì, A.; Leo, G.; Vasanelli, L.; Manna, L. Exciton relaxation processes in colloidal core/shell ZnSe/ZnS nanocrystals. *Appl. Phys. Lett.* **2003**, *82*, 418–420.
[45] Lad, A. D.; Mahamuni, S. Effect of ZnS shell formation on the confined energy levels of ZnSe quantum dots. *Phys. Rev. B* **2008**, *78*, 125421.
[46] Jang, E.; Kim, T.; Chung, H.; Choi, S. M.; Won, Y. H.; Lee, J. Y. Effect of tellurium doping on optoelectronic properties of blue ZnTeSe quantum dots. Research Square. Preprint (Version 1), January 26, 2022. Available from https://doi.org/10.21203/rs.3.rs-1183117/v1 (accessed Month Day, Year).
[47] Jin, W. X.; Deng, Y. Z.; Guo, B. B.; Lian, Y. X.; Zhao, B. D.; Di, D. W.; Sun, X. W.; Wang, K.; Chen, S. M.; Yang, Y. X. et al. On the accurate characterization of quantum-dot light-emitting diodes for display applications. *npj Flex. Electron.* **2022**, *6*, 35.